IEEE Robotics and Automation Letters (RA-L) paper, presented at ICRA 2026, Vienna, Austria. Cite as RA-L paper.

Design of wheel grouser geometry with reduced sinkage for LEV-1 lunar rover

Masatsugu Otsuki[1], Kent Yoshikawa[1], Takao Maeda[2], Naoto Usami[1], Tetsuo Yoshimitsu[1]

***Abstract*—Surface-mobile platforms have explored the moon and the red planet for nearly half century, providing a wealth of scientific data. However, surface mobility on planetary bodies remains a challenging task. In this paper, the formulation of reaction force by a grouser with a generalized geometry for a wheel of a planetary rover is presented, along with its verification through comparisons with the results by the conventional geometry. In a simulation study, the resistive force theory is applied to a general grouser geometry model. The study determines the impact of several parameters, particularly the grouser inclination, on draw-bar pull. The results obtained from the study suggest the formulation of a design for the grouser that is nearly optimal in its capacity to maximize the draw-bar pull per sinkage. We also apply the proposed geometry to the wheel on LEV-1, demonstrating that it works well in actual lunar operations.**

***Index Terms*—Space Robotics and Automation, Wheeled Robots, Dynamics**

I. Introduction

MOBILITY in planetary exploration is increasingly used for surface access, surface area coverage for *in situ* measurements, and access to scientifically intriguing sites that often occupy terrains with challenging topographies. Different research programs have investigated numerous mobility modalities, including several deployed by flight programs. To date, however, most of these modalities are constructed on wheeled platforms that are simple, energy-efficient, and which reduce the overall risk of their corresponding missions. Planetary surface mobility dates back to the late 1960s and early 1970s when the Soviet Union's unmanned lunar rovers Lunokhod [1] and the U.S.'s lunar roving vehicles [2] of the Apollo missions were operated on the lunar surface. More recently, not only rovers such as China's Jade Rabbit [3] and India's Pragyan [4] have briefly operated on the lunar surface, but also several rovers by private companies have been launched, and it appeared to be near to succeed in the operation. Meanwhile, NASA's Sojourner [5], Spirit, Opportunity [6], Curiosity [7] and Perseverance [8] rovers and China's Zhurong rover [9] have been roaming the red Martian surface. Further, France and Germany have announced their intention to launch the four-wheeled rover IDEFIX in 2026 as part of the Martian Moons Exploration mission [10].

Manuscript received: January 28, 2025; revised: March 15, 2025; accepted: April 4, 2025.

This paper was recommended for publication by Editor Lucia Pallottino upon evaluation of the Associate Editor and Reviewers' comments.

[1]M. Otsuki, K. Yoshikawa, N. Usami and T. Yoshimitsu are with Japan Aerospace Exploration Agency, Japan, otsuki.masatsugu@jaxa.jp

[2]T. Maeda is with Tokyo University of Agriculture and Technology, Japan, t-maeda@go.tuat.ac.jp

Mobility modalities other than wheeled platforms include the Soviet Union's ski-walker of the ill-fated Mars 2 mission [11], hoppers such as the PrOP-F Phobos platform [12], which move on low-gravity bodies, asteroid tumblers such as MASCOT, developed by the German Aerospace Center [13], robotic lander such as Philae, developed by the European Space Agency [14], and hybrid mobility platforms combining multiple modalities such as rolling and hopping [15]. On bodies with denser atmospheres such as Venus and Titan, balloon and other above-surface mobility modalities are preferred. In Japan, small celestial bodies have been explored by the hoppers called MINERVA [16], and they have taken many images that no one has ever seen. On the other hand, the SLIM spacecraft successfully landed on the Moon in January 2024 [17]. The Lunar Excursion Vehicle 1 (LEV-1) [18] and Lunar Excursion Vehicle 2 (LEV-2) [19] rovers were deployed when the SLIM spacecraft's back injection was stopped shortly before landing, and the operation continued for approximately 2 hours. LEV-1 demonstrates a new movement form of translational hopping and attitude/azimuth control by a single wheel. Following this, a large rover is planned to explore water resources on the Moon, and a moving mechanism using four crawlers was adopted [20].

Planetary rovers must survive the harsh environment of space. The thin or absent atmosphere exposes them to intense cosmic radiation, thermal cycling, and thermal extremes. In some cases, rovers must also contend with low gravity levels and unpredictable terrain properties, ranging from hard surfaces to sandy dunes, and from friable materials to sharp-edged, wind-eroded rocks. Low-gravity testing of mobility platforms is particularly difficult in terrestrial gravity-free testbeds because the testbed terrain is subject to Earth's gravity. Although the testbed regolith can be fluidized by airflow, this approach cannot accurately replicate the regolith conditions on small bodies. As a result, microgravity testing is limited to a few important experiments under well-defined conditions, and planetary exploration continues to rely on models and simulations that help us better understand terrain-contact interactions. For this purpose, researchers have simulated granular media under appropriate gravity levels of regolith [21]; however, this field is still in its infancy, and the types and heterogeneity of granular media that can be modeled by state-of-the-art simulation methods are limited. In recent years, it has been confirmed that the mechanical properties of the regolith surface on the planet have little dependence on gravity in terms of ultimate bearing capacity [22] and frictional force [23], and that partial design verification is possible even under Earth's gravity. The most unfavorable verification scenario, in which low gravity tests, ground tests,

IEEE Robotics and Automation Letters (RA-L) paper, presented at ICRA 2026, Vienna, Austria. Cite as RA-L paper.

and simulations are integrated, appears to be a critical component of quality assurance prior to the implementation of countermeasures during operational activities following the arrival at a target body.

In the past rovers, they suffered from wheel stacking and high slip on a loose soil, and it appeared to be a consequence of an increase in sinkage, which was a result of an increase in draw-bar pull. This suggests that the draw-bar pull could not be obtained without a certain degree of sinkage, while it was necessary to travel by holding the sinkage amount. Despite the fact that a larger wheel reduces the ground pressure, thereby decreasing sinkage amount and reducing the contact angle between the wheel and regolith surface, the large wheel increases both the mass and packaging requirements; they are generally avoided in flight rover designs. Consequently, there is a high demand for a wheel capable of generating substantial draw-bar pull while concurrently mitigating the amount of sinkage by a wheel whose envelope region remains constant. Therefore, reaction force calculations based on sinkage amount and a grouser design by a ground test are considered a viable solution.

The objective of our research endeavors is to ascertain grouser geometries that enhance mobility performance while minimizing sinkage and maintaining a constant installation envelope. This paper subsequently presents the findings from the implementation of the wheel on LEV-1, along with a practical demonstration of its functionality on the lunar surface. In Section II, the Resistive Force Theory (RFT) [24] is extended to a generalized grouser geometry, thereby formulating its reaction force. In Section III, the mission of LEV-1 is introduced, and the functions required for the wheel are mentioned. In Section IV, the range of the grouser's design examination is restricted, and the candidates for the grouser shape, which can anticipate the increase of draw-bar pull while the sinkage is mitigated, are presented. Subsequently, the near-optimal wheel grouser geometry is designed through a combination of single-wheel tests and Distinct Element Method (DEM) analysis. This design is then utilized in the context of the flight model manufacturing process. Section V presents the outcomes of verifying the realization of the required function on the lunar surface and Lessons Learned. The conclusions and future works are presented in Section VI. Throughout the remainder of this article, we replace the accurate planetary term regolith with soil, which is more familiar to readers. Strictly speaking, soil implies the presence of organics but not regolith.

II. Numerical model of wheel grouser geometry

Over the past half century, researchers have developed empirical models based on extensive experimental data [25]–[30]. In the 1960s, Bekker conducted sinkage experiments on a long flat plate and developed models pertaining to the stress on the plate due to sinkage. Empirical models provide adequate approximations for wheels with diameters in excess of 0.5 [m]; however, these models are inadequate for smaller wheels. More recently, Griffith and Spenko [31] developed a modified wheel-sinkage model for smaller wheel diameters.

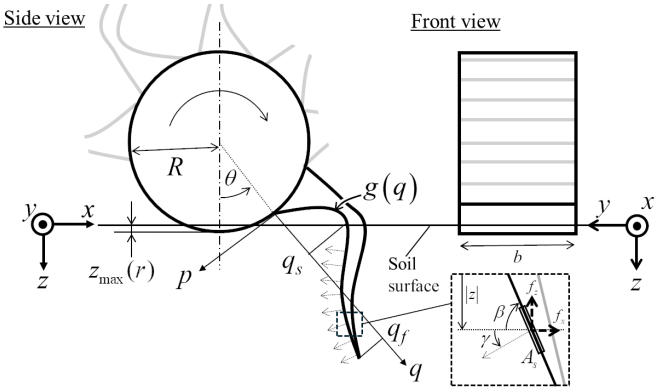

Fig. 1. Schematic of interaction model of wheel grouser geometry

However, these models require *a priori* understanding of the terra-mechanical properties, which are difficult to identify and can vary with terrain heterogeneity. As such, these models are constrained to characterizing the interaction under specific parameters and conditions, which precludes a comprehensive capture of the multifaceted interactions between the wheel and the ground. Therefore, approaches that would enhance our understanding of such complex interactions are worthy of further investigation. For example, Li et al. [24] developed an alternate approach to classical terra-mechanical models [25], [27] based on the resistive force model [32]. They measured the resistive force of a small plate moving freely through granular media and thus proposed the resistive force theory. The model reduces the number of tunable parameters from three, as in Bekker's model, to one, namely the scaling factor. RFT is an empirical model based on experimental results; consequently, its application has been limited to specific terrain types. Notwithstanding, the model is considered appropriate for a comparative analysis of different grouser geometries in the light of the partially-known terrain properties of planetary bodies. The RFT model is not dependent upon conventional terra-mechanical properties; therefore, it can effectively simulate the dynamic motions of a grouser wheel.

In our formulation, an arbitrary grouser geometry mounted on a wheel of arbitrary radius is parameterized by a curve. The grouser-soil interaction induces a pull on the draw-bar, which is modeled by RFT [24]. We here describe the grouser model and formulate its generated forces. The reaction or resistive force exerted on the wheel geometry is expressed as

$$f_{(z,x)} = \int_S \alpha_{(z,x)}(\beta, \gamma)\, |z|\, dA_s, \tag{1}$$

where α is the resistive stress per unit depth on a tiny surface patch dA_s, and z is the sinkage depth from the soil surface; and α has the different distribution in z and x directions, respectively. The stress is also a function of β, the attack angle between the tangential patch and the horizontal plane, and γ, the intrusion angle of the patch, as mentioned in the reference [24] and shown in Fig.1. $|z|$ is the patch's depth below the surface, and A_s is the area of the patch moving in the granular media. The lift f_z and drag f_x forces on the patch act in the vertical and horizontal directions, respectively.

We develop a generalized representation of a grouser shape, in which we model the grouser-soil interaction, as shown in

IEEE Robotics and Automation Letters (RA-L) paper, presented at ICRA 2026, Vienna, Austria. Cite as RA-L paper.

Fig.1. The resistive force exerted on the grouser's surface can be described by Eq.(1), which also calculates the resistive force exerted on a grouser. Consider a grouser shape $g(q)$, expressed in terms of the grouser coordinate axis q. The grouser surface element dA_s and its sinkage depth z are then rewritten as

$$dA_s = b\sqrt{1+\left[\frac{dg(q)}{dq}\right]^2}\,dq, \tag{2}$$

and

$$z = [R+q]\cos\theta + g(q)\sin\theta - [R - z_{\max}]. \tag{3}$$

where b is the width of the wheel, R is the wheel radius, z_{max} is the wheel rim sinkage, and θ is the rotational angle at the base of the grouser. As mentioned above, if the sinkage z is negative (as for parts of the grouser lying above the soil surface) or zero, it is set to zero; that is, the grouser does not contact or interact with the surface.

The resistive stress parameters β and γ are respectively written as:

$$\beta = \begin{cases} -\frac{\pi}{2} - \theta + \tan^{-1}\left(\frac{dg(q)}{dq}\right), \theta \in \left[-\frac{\pi}{2}, 0\right] \\ \frac{\pi}{2} - \theta + \tan^{-1}\left(\frac{dg(q)}{dq}\right), \theta \in \left[0, \frac{\pi}{2}\right] \end{cases}, \tag{4}$$

and

$$\gamma = \theta - \tan^{-1}\left(\frac{dg(q)}{dq}\right) + \eta, \tag{5}$$

where η is determined by the rotational speed of the wheel; however, for this object, the value of η is negligible, amounting to a few degrees per second. Substituting Eqs.(2) and (3) for dA_s and z respectively in Eq.(1), the equation of the grouser resistive force f_g in the z and x directions becomes

$$f_{g(z,x)} = b\int_{q_s}^{q_f} \alpha_{(z,x)}(\beta,\gamma)\{[R+q]\cos\theta + g(q)\sin\theta - [R - z_{\max}]\} \times \sqrt{1+\left[\frac{dg(q)}{dq}\right]^2}\,dq\,, \tag{6}$$

where $[q_s, q_f]$ represents the portion of the grouser geometry along the grouser axis q that contacts the soil. The end point, q_f, is typically the point of the grouser farthest from the center of the wheel. To obtain the submerged starting point of the grouser, q_s, we solve the following equation:

$$q_s - q_z + g(q_s)\tan\theta = 0, \tag{7}$$

where q_z is the submerged starting point on the q coordinate axis, which is geometrically calculated as follows:

$$q_z = \frac{R - z_{max}}{\cos\theta} - R. \tag{8}$$

III. LEV-1

The LEV system was installed on the SLIM spacecraft, which was launched from Japan in September 2023. The LEV system comprised the following components: LEV-M, LEV-1 (Fig.2), and LEV-2 [19]. The primary objective of LEV-1 was to execute an engineering demonstration of a novel mobility mechanism and autonomous functionality under low-gravity conditions; additionally, it was responsible for recording the status of the SLIM spacecraft and the designated landing site. The installation of LEV was determined during the critical design phase, when the mass margin was defined. Therefore, the SLIM spacecraft had a simple interface to the LEV system, which consisted of a power source and a thermal control system; the LEV mass and dimensions were also required to be as small as possible. The LEV-1's operational design was characterized by its autonomy, direct communication with the ground station, and solar cell-based power supply; specifically, LEV-1 became independent from the SLIM spacecraft following its deployment [18]. LEV-1 was launch-locked by two Hold Down Release Mechanisms (HDRMs), and at the start of a free fall after stopping the back injection of the SLIM spacecraft, LEV-1 was deployed by extruding it with a spring along with the activation of HDRMs. Furthermore, although LEV-1 was a hopping-type exploration robot comparable to MINERVA, which were designed for the exploration of small bodies, it was engineered to facilitate mobility in multiple directions via azimuth control, enabled by a single wheel.

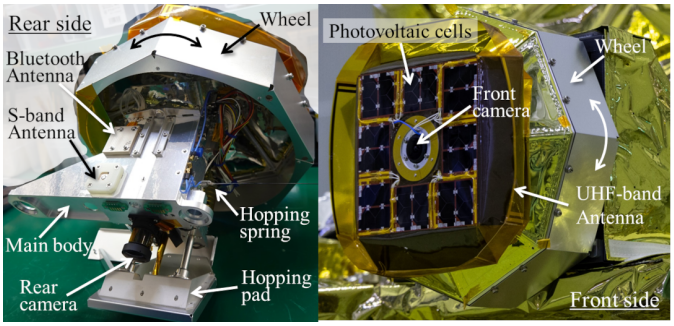

Fig. 2. LEV-1 flight model rear view (left) , front view installed on the SLIM spacecraft (right) and description of the main components

As shown in Fig.2, the hardware of LEV-1 comprised solar cells, photo diodes, rechargeable batteries, front and rear cameras, communication antennas, a hopping pad that functions as a moving mechanism, and a wheel. The mass of LEV-1 was approximately 2.1 [kg], the wheel diameter was approximately 300 [mm], and the length was approximately 400 [mm] in the most extended state. The LEV-1 system was equipped with a 3-axis accelerometer, a 3-axis gyroscope, an impact accelerometer, a radiation dosimeter, thermometers, and direct communication capability with the ground station in S/UHF-band and with the LEV-2 system via Bluetooth.

LEV-1 possessed the capacity for linear movement and azimuth control in any direction by the combination of hopping and wheel rotation. It was imperative to regulate the attitude through the rotation of the wheel, given that the attitude in the gravity direction significantly deteriorated following the deployment from the SLIM spacecraft and the hops. This approach involved the control of three axes: the direction of solar cells towards the Sun, the orientation of the camera towards an arbitrary target, the antenna for communication with Earth, and taking a hopping attitude.

As shown in Fig.3, the transition occurs from the attitude inversion state in the direction of gravity to a state in which the

IEEE Robotics and Automation Letters (RA-L) paper, presented at ICRA 2026, Vienna, Austria. Cite as RA-L paper.

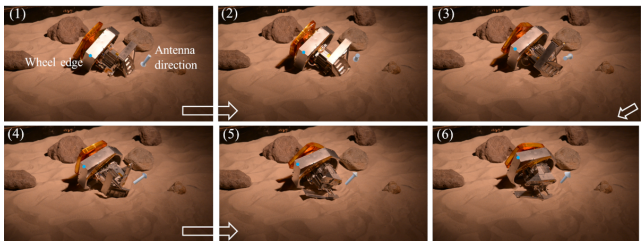

Fig. 3. Flow of attitude recovery control by wheel rotation

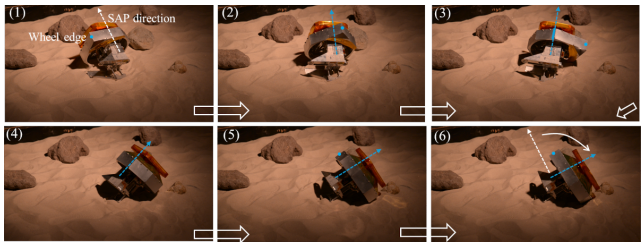

Fig. 4. Flow of azimuth control by wheel rotation

S-band antenna is rotated upward by the wheel. In contrast, as illustrated in Fig.4, the direction of the solar cells undergoes a 90-degree alteration due to the rotation of the wheel. Although the attitude control was implemented by the wheel rotation, as evidenced by the figures, it was sequenced in the order of the azimuth control from the attitude control. This was not random, but rather was a consequence of the disparity in rotational resistance between the wheel and the rover body. In the event of an attitude inversion, the rotational resistance of the wheel was increased, causing the rover body to rotate. When the attitude in the gravity direction becomes normal, the hopping pad, which is attached to the rover body, generates substantial rotational resistance, causing the wheel to rotate. The design of a single wheel constituted a pivotal technology for the survival of the rover on the lunar surface, necessitating the mitigation of problems such as wheel stacking and insufficient draw-bar pull, which have plagued earlier rovers. In this study, the wheel grouser geometry was designed by using the model from the previous section; this approach was employed to achieve a distinctive grouser shape that could anticipate substantial draw-bar pull while concurrently minimizing sinkage.

IV. Wheel Grouser Geometry Design for LEV-1

A. Evaluation of design of a grouser

This section provides details of the grouser shape design for the wheel of LEV-1. The majority of conventional rovers were equipped with wheels that feature flat and rectangular grousers. The wheel was generally formed as a barrel shape [6] or carved with a distinctive chevron pattern on the wheel rim [7]. Since there are many possible solutions for the grouser shape design, the design scope is narrowed to obtain a realistic solution. First, since the wheel of LEV-1 does not need to steer, but only to rotate, it was supposed that the wheel rim has a simple cylinder shape. The chevron pattern was also omitted due to the relatively narrow width of the wheel. Furthermore, although there was some discussion [33] about the number of grousers per round, the verification in this paper was supposed to be nominally based on 24 grousers. Finally, the design for

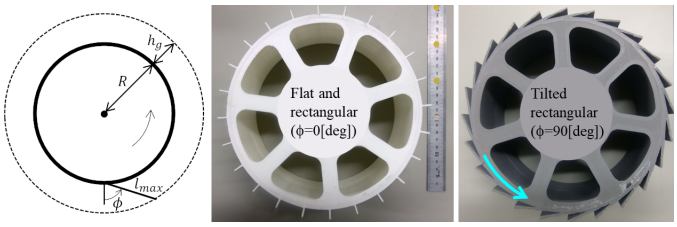

Fig. 5. Schematic of the wheel with a rectangular grouser (left), and the exterior views of the tested wheels: (center) with flat and rectangular grousers and (right) with rectangular grousers tilted at 90 [deg]

the grouser was based on a flattened grouser that enters the envelope, and the grouser shape design was replaced by the problem of optimizing the angle and length of the grouser.

Figure 5(left) illustrates the hypothesized shape of the grouser and its corresponding dimensional relationship. Here, the entire grouser configuration is assumed to lie within the circle with binding radius $R+h_g$. h_g is the height of the grouser. According to Eq.(6), the reaction force of a grouser sinking into the soil is calculated. The shape function of the flat and rectangular grouser inclined at angle ϕ from the q coordinate axis is calculated as

$$g(q) = q\tan\phi, \quad \frac{dg(q)}{dq} = \tan\phi. \tag{9}$$

And the starting point q_s and the end point q_f of the submerged grouser are derived from the followings, respectively.

$$q_s = \frac{q_z}{1+\tan\phi\tan\theta}, \quad q_f = l_{max}\cos\phi, \tag{10}$$

where l_{max} is the maximum grouser length within the radius-bound $R+h_g$ given by,

$$l_{max} = -Rcos\phi + \sqrt{h_g^2 + 2h_gR + R^2cos^2\phi}. \tag{11}$$

With Eq.(6) and the parameters, $R = 100$ [mm], $h_g = 10$ [mm], $b = 100$ [mm], the profile of the generated force by a grouser against the rotational angle around the fixed center of the wheel are calculated as Figs.6 and 7. In this instance, the scaling factor is designated as 1. Figure 6 shows the results of force $f_{g(x)}$ generated in forward direction at each grouser angle, and Fig.7 shows those of force $f_{g(z)}$ generated on the direction of gravity at each grouser angle. The results in Fig.6 show that the wheel with the grouser of almost 90-degree lying down provides the greatest forward force as long as the vertical position of the wheel remains the same. Figure 7 also shows that the force of lifting from the ground is greatest, i.e., it is the easiest grouser to move forward in a floating state. It is predicted that the result will be a draw-bar pull with less sinkage, a phenomenon that should be experimentally validated.

B. Verification through single wheel tests

The traveling performances of the wheel with 90-degree tilted grousers extended to the maximum length in the envelope, which was characterized in the reaction force analysis of a single grouser, a wheel with common non-tilted grousers, and a wheel with 10-degree inclined grousers were evaluated in a single wheel testbed.

IEEE Robotics and Automation Letters (RA-L) paper, presented at ICRA 2026, Vienna, Austria. Cite as RA-L paper.

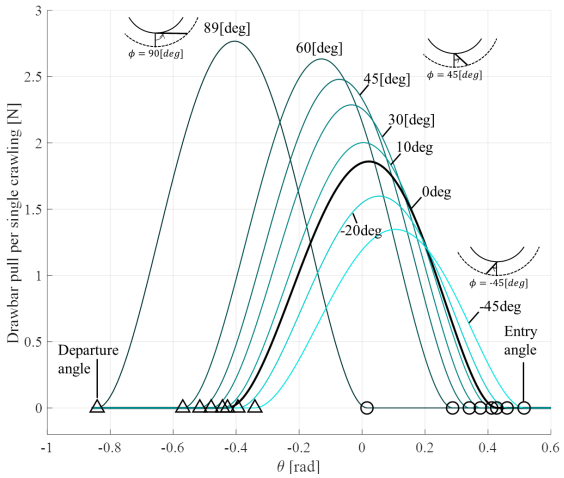

Fig. 6. Calculation of draw-bar pull based on the proposed model

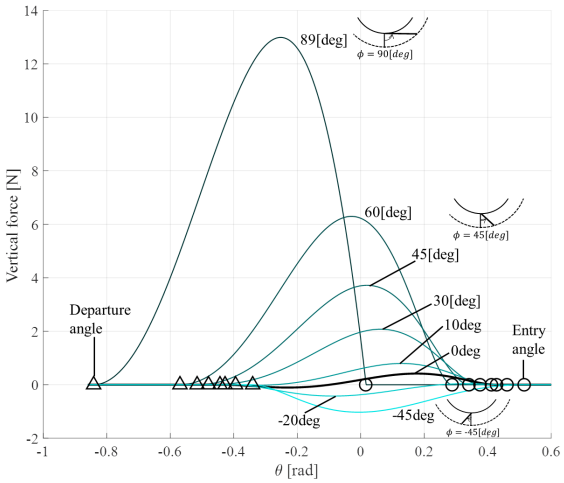

Fig. 7. Calculation of vertical force based on the proposed model

1) Single wheel testbed: All of the experimental grouser wheels were 3D printed using polylactide resins, as shown in Fig.5 (center and right). Each wheel was manufactured with adequate rigidity to support the grousers. The total mass of each wheel was with 0.32 $\pm$ 0.050 [kg]. The standard deviation negligibly affected the experimental results because the variation was below 1.0 % of the average vertical load (54 [N]). The nominal wheel radius R is 0.10 [m]. The addition of 24 grousers increases the wheel envelope height by 10 [mm]. In total, four wheels were fabricated for the experiments; three with rectangular grousers at different inclinations: $\phi = 0, 10, 90$ [deg]. The final wheel was a grouser-less wheel with a radius 110 [mm], which corresponded to the same bounding radius as the wheels equipped with grousers.

The experimental setup is illustrated in Fig.8. The wheels were attached to a drive motor with a double-stage gear train of planetary and harmonic gears. The base plate of the motor was affixed to a six-axis force-torque sensor. In turn, a wheel assembly was mounted on a linear vertical guide, thereby enabling unobstructed, low-friction movement along the z axis. The vertical linear guide, equipped with the wheel assembly, was mounted on a horizontal low-friction slide rail and driven by a load motor via a timing belt. The weight of the wheel assembly generated the vertical load of 54 [N] on the wheel. In this setup, the draw-bar pull, wheel sinkage and motor

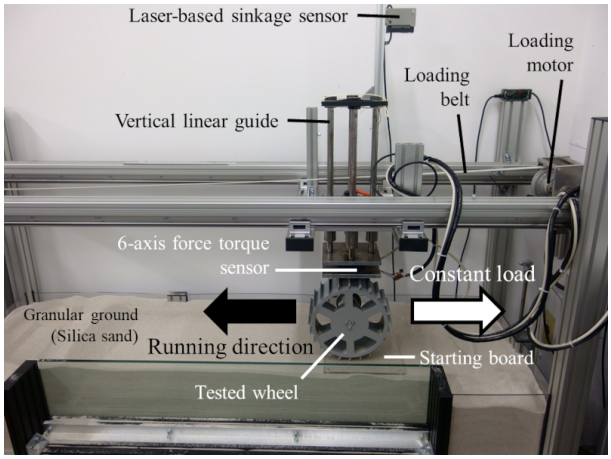

Fig. 8. Appearance of the single-wheel testbed

current were measured. The slip ratio was derived from the rotational angle and the linear position of the wheel measured by digital encoders attached to the motor and the horizontal linear guide, respectively. The wheel sinkage was measured by a laser-distance sensor located at the top of the vertical guide. To initialize the sensor, the wheel motion was started on a large rigid plate of known thickness and sinkage. In all experiments, the slip ratio was set to 10, 30, 50, or 70%, and it was controlled by the loading motor via the belt attached to the wheel axis. The time histories of the slip ratio, sinkage, draw-bar pull and current were synchronously measured. Each test was conducted in triplicate.

2) Sand properties for test: The granular medium used through the experiments was Tohoku silica sand No.5. As the properties of granular media are contingent upon environmental factors, such as air pressure and humidity, the sand properties were measured conccurently with the draw-bar pull experiments on the same day and within a brief interval. Prior to each run, the sand was meticulously manually fluffed up and flattened with a leveling plate. The scaling factor for the sand was measured according to the method described in [24]. On each experimental day, the pressure-sinkage relation was measured using a Rimik CP40II penetrometer. In these measurements, a flat circular tip-plate with a 330 [mm^2] cross section was employed. The tip-plate experiment was repeated until it penetrated 6 [cm] into the medium, requiring over 20 experimental runs to achieve this depth. From the tip-plate experiments, the average scaling factor of the tested sand was determined to be in the rage of 2.45–2.55, with a standard deviation that falls below 10 % of the predominant value.

3) Results of single wheel tests: Figure 9 presents the draw-bar pull of the three rectangular wheels and the grouser-less wheel, respectively, as a function of wheel rim sinkage. The slip ratio of the wheel motion, which must be controlled during traveling, was derived as 10, 30, 50, and 70 %, respectively, from the sinkage origin of the figure, as specified in Fig.9. Each cross-line at an arbitrary data point signifies the range of minimum and maximum values with regard to the slip ratio and the draw-bar pull. The rectangular grouser inclined at $\phi = 10$ [deg] performed similarly to the nominal flat grouser inclined at $\phi = 0$ [deg]. This result is consistent with the

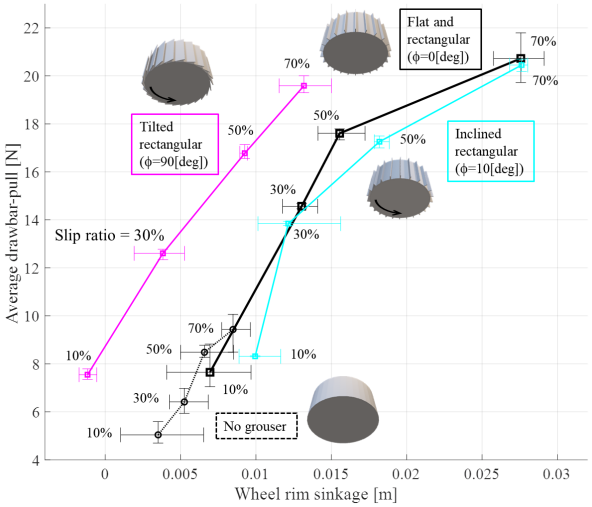

Fig. 9. Draw-bar pull generated by each tested wheel on sinkage

numerical results of the previous section (Fig.6), in which the performances of these two grouser types differed by less than 5%. Therefore, multiple experiments on these two grouser types yield consistent results, thereby confirming the good repeatability of the experiment. The grouser-less wheel achieved less sinkage and smaller draw-bar pull than the other wheel types, confirming that efficient traveling needs appropriate-spacing of grousers. Note that the draw-bar pull curve of the flat ($\phi = 0$ [deg]) grouser wheel overlaps and extends beyond the grouser-less wheel curve. At lower sinkage, the draw-bar pull of the wheel with the rectangular grousers tilted at $\phi = 90$ [deg] exerts the largest one among the inclined/tilted grouser designs. In Fig.9, the rectangular grouser tilted at $\phi = 90$ [deg] demonstrates minimal sinkage with increasing slip ratio. Consequently, the low sinkage decreases the motor current and mitigate the risk of entrapment in the loose soil ground.

Meanwhile, from the results in Fig.6, we expected several times more draw-bar pull by the grouser tilted at $\phi = 90$ [deg] when the slip ratio was the same, but it was almost the same as that by the other grousers. This could be attributed to the fact that the reaction force was calculated at a constant amount of sinkage; it was hypothesized that the large levitation force was generated in the wheel response, as illustrated in Fig.7, thereby reducing the amount of sinkage. Therefore, a thorough calculation of the sinkage amount is paramount; however, the calculation of reaction forces involving multiple grousers based on the sinkage amount is deficient. It was evident that there was a paucity of theoretical preparation at this stage, and it could be posited that it is imperative to continue evaluating the geometry design through experiments and numerical simulations.

C. Practical design for wheel geometry of LEV-1

The final design determined by verifying the traveling performance of the wheel with grousers was evaluated through the analysis using Altair EDEM, a commercial software that implements the DEM simulation. First, a single-wheel run with a constant load was conducted on a ground composed of particles of Tohoku silica sand No.5, which was utilized in the aforementioned tests; this sand achieves an angle of repose of 30 [deg]. As illustrated in Fig.10, the DEM simulation involves three wheels running within the gravitational field of the Moon; the experiment utilized the same wheels as in the study, incorporating 0, 10, and 90-degree inclined/tilted grousers. The results in Fig.11 elucidate the correlation between the wheel rim sinkage and the mean draw-bar pull under the five conditions with different loads side-by-side under Earth's gravity. It is obvious in Fig.11 that the same 90-degree grouser wheel as in the experimental results exhibited a substantial draw-bar pull with the minimal sinkage. The results presented in Fig.11 are derived with the primary aim of confirming that a similar trend to the results in Fig.9 emerges within a realistic calculation time, and the precise congruence between their results is not a prerequisite.

This simulator was subsequently utilized to assess the design for implementation of the LEV-1 wheel. It was reasonable to assume that a similar degree of traveling performance should be achieved regardless of the direction of travel. To that end, a polygonal wheel was designed (Fig.12) by arranging 8, 12, and 24 90-degree tilted grousers on the wheel rim in a mirror-image relation. Thereafter, the performances were compared using the DEM analysis, as illustrated in Fig.12. It was evident that a substantial draw-bar pull was generated with a reduced sinkage, and the sinkage remained constant even under substantial loads. However, this did not result in an increase in sinkage because the sand was not transported when slip increased. Nevertheless, the traveling efficiency was found to be poor, as shown in Fig.12.

In conclusion, the wheel grouser geometry of the flight model was decided to be an octagonal shape, given its capacity to maintain the draw-bar pull with minimal sinkage and its manufacturability. Since the octagonal shape has fewer corners than other polygons, it can be manufactured by sheet metal processing, resulting in a thinner plate than other polygonal wheels that need cutting works. Consequently, we were able to reduce all the costs associated with manufacturing, processing time, and especially mass increase. Depending on the marginal mass of the SLIM spacecraft, LEV-1 was a device that could be ridden, meaning that mass control was strict. In the case of the octagonal wheel, the grouser part could be manufactured using a 0.3 mm-thick plate weighing approximately 60 grams; however, in the case of machined wheels, a significantly higher mass would be required, and the mass would exceed the permissible limit. On the Tohoku silica sand No.5 ground, it was ascertained that the attitude and azimuth controls functioned without complications, as evidenced in Figs.3 and 4, and the octagonal wheel grouser geometry was implemented on LEV-1.

V. The Operation Results on the Lunar Surface

A. The results on wheel control of LEV-1

On January 19, 2024 UTC, just before the SLIM spacecraft landed on the Moon, LEV-M deployed LEV-1 and LEV-2 independently to the lunar surface [17]. After the deployment, LEV-1 performed 7 times of hopping operation, while observing environmental state by optical cameras and temperature

IEEE Robotics and Automation Letters (RA-L) paper, presented at ICRA 2026, Vienna, Austria. Cite as RA-L paper.

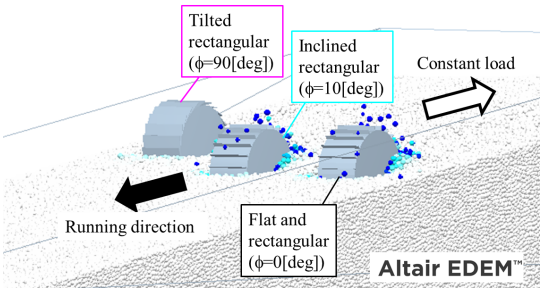

Fig. 10. Calculation conditions for DEM analysis with 3 wheels in the lunar gravitational environment

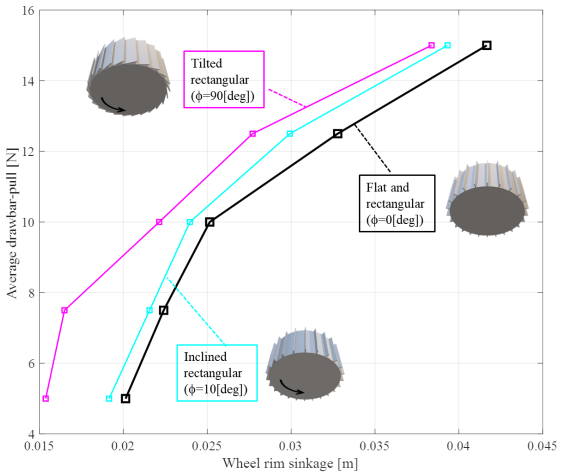

Fig. 11. DEM Analysis results for the same conditions as the single-wheel test in the Earth's gravitational field

sensors, and attitude control was autonomously carried out in the interval. Figure 13 illustrates the timing of the transmission of the LEV-1 S-band radio signals with 1 second period; however, the time step of house keeping data derived from the demodulated data was very coarse. The S-band antenna is attached to the back of LEV-1; hence, no radio signal can physically reach the ground station when LEV-1 is inverted after the hop or landing. LEV-1 is equipped with an algorithm that automatically orientates the S-band antenna towards the ground station by controlling its attitude. In the event that this is not feasible, the system will stop to transmit S-band radio signals. Consequently, the S-band radio signals were observed to return on numerous occasions, thereby indicating that the attitude recovery control by the wheel was completely performed.

Figure 14 illustrates the absolute ratio of the transmitted power of the left- and right-handed circular polarization (LHCP and RHCP) radio signals emitted from the front and back surfaces of the UHF film antenna, respectively. The transmission power of each LHCP/RHCP is contingent upon the earthward component of the antenna's directivity. The alteration in directivity is observed only in instances where the dielectric configuration surrounding the antenna undergoes a change or when the earth direction undergoes a shift due to a variation in the LEV-1's azimuth. In the context of LEV-1 on the lunar surface, the event that triggered a significant alteration in the ratio between LHCP and RHCP was a change in the direction of the Earth; hence, a change in the ratio must

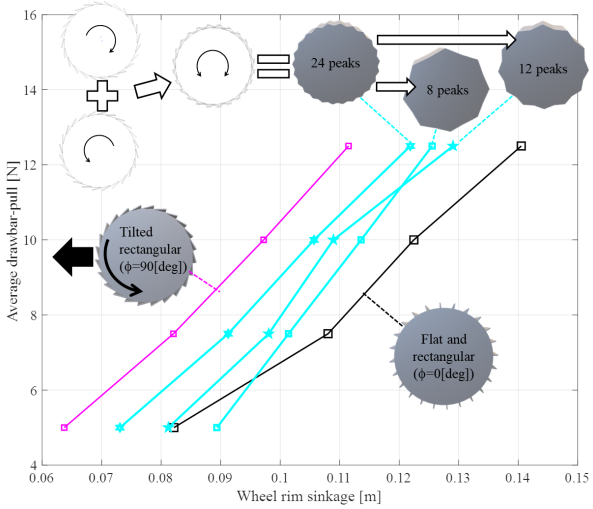

Fig. 12. Performance evaluation by the DEM analysis of the proposed wheel grouser geometry under the lunar gravity

be considered to be equivalent to a change in the azimuthal orientation of the antenna relative to the Earth. Consequently, during the period in which the amplitude of the ratio varied, the wheel actually caused a change in heading, with the exception of the hop.

As the result, LEV-1 demonstrated the capacity to sustain operation on the lunar surface for approximately 2 hours by directly transmitting recorded data, including images, to the ground station without the involvement of the SLIM spacecraft. A series of actions were executed autonomously, without human intervention from the ground station. Furthermore, the communication between LEV-1 and LEV-2 on the lunar surface was accomplished for the first time in the world. Consequently, LEV-1 became Japan's first lunar exploration robot, and it became the world's first hopping mobile robot. In addition, LEV-1 employed the amateur radio UHF band for another data transmission from the lunar surface, establishing the first lunar amateur radio station. This pioneering achievement was a major milestone in the field, enabling widespread participation in space exploration.

B. Leassons Learned of the geometry design

After developing a wheeled rover with low resources such as LEV-1, we obtained the following Leassons Learned.

- By circumventing the intricacies inherent in the grouser shape of the wheel, it becomes feasible to mitigate manufacturing constraints and reduce weight.
- It is imperative to optimize the balance of vertical and lateral reaction forces in order to obtain the wheel geometry that generates the anticipated draw-bar pull.
- Empirical models, rooted in experimental findings, and numerical simulations, such as DEM, remain imperative for the verification of the wheel geometry designs of planetary rovers.

VI. Conclusions

We presented the reaction force analysis model of the single grouser and showed the geometry design results for LEV-1.

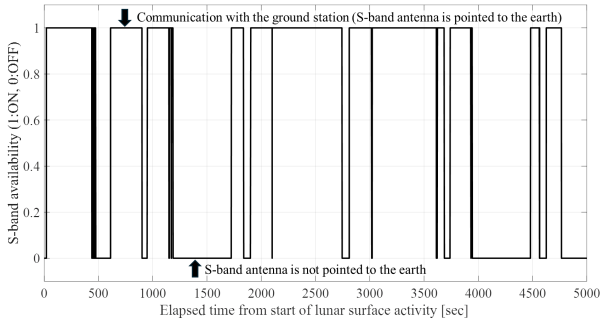

Fig. 13. Grounds of attitude control by the wheel rotation on lunar surface

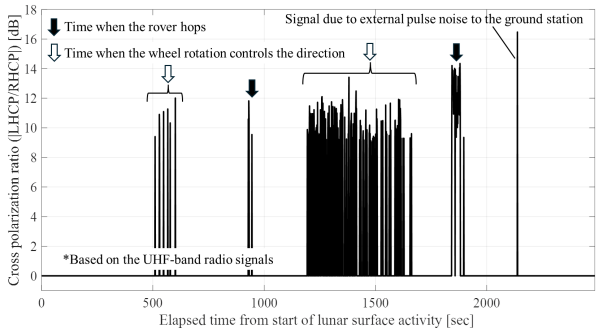

Fig. 14. Grounds of azimuth control by the wheel rotation on lunar surface

And, this paper presented not only evaluation results by the ground test and analysis but also that LEV-1 conducted normal operation on the lunar surface. The following two points were revealed in this paper. First, the proposed analysis model introduced the grouser shape that was capable of generating the substantial draw-bar pull with the minimal amount of sinkage; this was subjected to both experimental and analytical evaluations to demonstrate its effectiveness. Next, the wheel grouser geometry, which was designed on the basis of the analysis assuming low gravity, was mounted on LEV-1 and its functionality was demonstrated on the lunar surface. The certain compromises were ultimately made with regard to performance, specifically in terms of ease of mounting and manufacturing it. In particular, given that the primary objective was to reduce the amount of sinkage, the reaction force in the upward direction was occasionally excessive, while the draw-bar pull was insufficient.

The challenge for the future is to design a grouser that can always both suppress sinkage and increase draw-bar pull under some constraints. Furthermore, it is imperative to examine the precision of the grouser model and establish a calculation method of a reaction force by multiple grousers. Finally, the success in controlling the rotation of the wheel made it possible to provide a small, inexpensive robot for lunar exploration, and this robot was considered suitable for a future multi-robot areal exploration.

ACKNOWLEDGMENT

The authors are grateful to Dr. Issa A.D. Nesnas of JPL for inspiring us to find new geometry in the design of a wheel grouser, continuing interest and encouragement. The authors are also grateful to Dr. Genya Ishigami who offered the use of his facility for the single wheel test.

REFERENCES

[1] D. Carrier, "Soviet rover systems," in *Proc. AIAA Space Programs and Technologies Conference*, 1992.
[2] B. Burkhalter *et al.*, "Lunar roving vehicle: historical origins, development and deployment," *J. the British interplanetary society*, vol. 48, 1995.
[3] E. Lakdawalla, "China lands on the moon," *Nature Geoscience*, vol. 7, no. 81, January 2014.
[4] T. V. Padma, "India's moon mission: four things chandrayaan-3 has taught scientists," *Nature*, vol. 621, no. 456, 2023.
[5] B. Wilcox *et al.*, "Sojourner on Mars and lessons learned for future planetary rovers," SAE Technical Paper, Tech. Rep., 1998.
[6] S. W. Squyres *et al.*, "Athena Mars rover science investigation," *J. Geophysical Researchs*, vol. 108, no. E12, p. 8062, 2003.
[7] R. Welch *et al.*, "Systems engineering the Curiosity rover: A retrospective," in *Proc. 2013 8th International Conference on System of Systems Engineering*. IEEE, June 2013, pp. 70–75.
[8] V. Verma *et al.*, "Autonomous robotics is driving perseverance rover's progress on mars," *Science Robotics*, vol. 8, no. 80, 2023.
[9] C. Li *et al.*, "Layered subsurface in utopia basin of mars revealed by zhurong rover radar," *Nature*, vol. 610, pp. 308–312, 2022.
[10] Y. Kawakatsu *et al.*, "Preliminary design of martian moons exploration (mmx)," *Acta Astronautica*, vol. 202, pp. 715–728, 2023.
[11] P. Ulivi and D. M. Harland, *Robotic exploration of the solar system, Part 1: The Golden Age 1957-1982*. Chichester: Springer, 2007.
[12] S. Ulamec *et al.*, "Hopper concepts for small body landers," *Advances in space research*, vol. 47, no. 428, 2011.
[13] R. Jaumann *et al.*, "A mobile asteroid surface scout (MASCOT) for the Hayabusa 2 mission to 1999 JU3: The scientific approach," in *Proc. 44th Lunar and Planetary Science Conference*, 2013.
[14] S. Ulamec *et al.*, "Rosetta lander – Philae: Implications of an alternative mission," *Acta Astronautica*, vol. 58, pp. 435–441, 2006.
[15] B. H. Wilcox *et al.*, "The MUSES-CN nanorover mission and related technology," in *Proc. 2000 IEEE Aerospace Conference*, 2000.
[16] T. Yoshimitsu, "Development of autonomous rover for asteroid surface exploration," in *Proc. International Conference on Robotics and Automation 2004*, 2004, pp. 2529–2534.
[17] L. Xin, "Japan' s successful moon landing was the most precise ever," *Nature*, vol. 626, pp. 18–19, 2024.
[18] T. Yoshimitsu *et al.*, "Small hopping robot for lunar exploration," in *Proc. 74th International Astronautical Congress*, 2023.
[19] D. Hirano *et al.*, "Transformable nano rover for space exploration," *IEEE Robotics and Automation Letters*, vol. 9, no. 4, pp. 3139–3146, 2024.
[20] H. Mizuno *et al.*, "Project status on lunar polar exploration (LUPEX) mission," in *Proc. 74th International Astronautical Congress*, 2023.
[21] S. Wakabayashi *et al.*, "Design and mobility evaluation of tracked lunar vehicle," *J. Terramecanics*, vol. 46, no. 3, pp. 105–114, 2009.
[22] T. Kobayashi *et al.*, "Bearing capacity of shallow foundations in a low gravity environment," *Soils and Foundations*, vol. 49, no. 1, pp. 115–134, 2009.
[23] M. Sutoh *et al.*, "Surface sliding behavior analysis of space probes in simulated extraterrestrial environments," in *Proc. IEEE International Conference on Intelligent Robots and Systems*, 2021, pp. 8774–8781.
[24] C. Li *et al.*, "A terradynamics of legged locomotion on granular media," *Science*, vol. 339, pp. 1408–1412, March 2013.
[25] M. G. Bekker, *Off-The-Road Locomotion*. University of Michigan Press, 1960.
[26] A. R. Reece, "Principles of soil – vehicle mechanics," in *Proc. the Institution of Mechanical Engineers, Automobile Division 1947-1970*, vol. 180, 1965, pp. 45–66.
[27] J. Y. Wong, *Terramechanics and Off-Road Vehicles*. Elsevier Science Publisher, 1989.
[28] M. Sutoh, "Traveling performance analysis of lunar/planetary robots on loose soil," Ph.D. dissertation, Tohoku University, March 2013.
[29] L. Ding *et al.*, "Interaction mechanics model for rigid driving wheels of planetary rovers moving on sandy terrain with consideration of multiple physical effects," *J. Field Robotics*, August 2014.
[30] F. Zhou *et al.*, "Simulations of Mars rover traverses," *J. Field Robotics*, vol. 31, no. 1, pp. 141–160, 2014.
[31] G. Meirion-Griffith and M. Spenko, "A modified pressure-sinkage model for small, rigid wheels on deformable terrains," *J. Terramechanics*, vol. 48, no. 2, pp. 149–155, April 2011.
[32] J. Lighthill, *Mathematica Biofluiddynamics*. SIAM, 1975.
[33] H. Inotsume *et al.*, "Analysis of grouser performance to develop guidelines for design for planetary rovers," in *Proc. i-SAIRAS 2014*, 2014.